ACS Energy LETTERS

http://pubs.acs.org/journal/aelccp

LETTER

Fastening Br^- Ions at Copper–Molecule Interface Enables Highly Efficient Electroreduction of CO_2 to Ethanol

Jianghao Wang,[§] Hao Yang,[§] Qianqian Liu, Qian Liu, Xiaotong Li, Xiangzhou Lv, Tao Cheng,* and Hao Bin Wu*

Cite This: *ACS Energy Lett.* 2021, 6, 437–444

Read Online

ACCESS | Metrics & More | Article Recommendations | Supporting Information

ABSTRACT: **Developing advanced electrocatalysts to convert CO_2 into liquid fuels such as ethanol is critical for utilizing intermittent renewable energy. The formation of ethanol, however, is generally less favored compared with the other hydrocarbon products from Cu-based electrocatalysts. Herein, we construct an efficient electrocatalyst for ethanol formation based on dodecanethiol-modified CuBr, which *in situ* generates a robust Br-doped Cu–thiol interface. The obtained electrocatalyst shows a significantly enhanced C2+ Faradaic efficiency of 72%, among which the Faradaic efficiency of ethanol is 35.9%. Notably, the ratio of ethanol to ethylene significantly increases from 0.32 for pristine CuBr to 1.08 for dodecanethiol-modified CuBr. The improved electrocatalytic activity is related to the modulated adsorption energy of key intermediates on the Br-doped Cu–thiol interface as verified by density functional theory (DFT) calculations. The present study highlights the great potential of utilizing hybrid metal–molecule interfaces for improving electrocatalytic CO_2 conversion.**

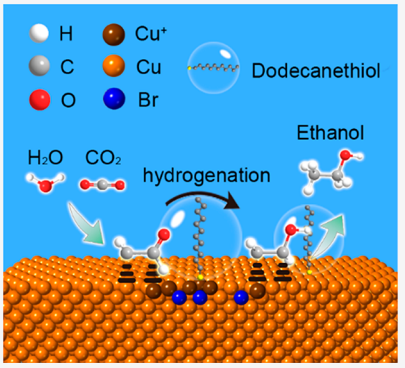

CO_2-neutral economics are in demand because of climate change and the environmental crisis associated with excessive exploitation of fossil fuels. Electrochemically reducing CO_2 by renewable electricity offers a feasible approach to sustainably obtain value-added feedstocks (e.g., ethylene) and dispatchable liquid fuels (e.g., ethanol).[1−3] Developing advanced electrocatalysts with high activity and selectivity toward target products plays a key role in the implementation of CO_2 electroreduction technology, which remains a great challenge.

To date, Cu-based electrocatalysts are the only options to catalyze the CO_2 reduction reaction (CO_2RR) to multicarbon products with noticeable selectivity. However, selectivity toward a specific oxygenate, such as ethanol, remains low, while the competing hydrogen evolution reaction (HER) further worsens the situation.[4] The CO_2RR product distribution of Cu-based electrocatalysts highly depends on factors such as morphology, microstructure, and composition.[5,6] Thus, finely tuning the electrode interface offers the opportunity to boost the catalytic performance toward desirable products. For example, Cu-based electrocatalysts derived from CuBr are promising for selective C−C coupling.[7] CuBr as precatalyst can be electrochemically transformed into nanoarchitectures with a high degree of roughness, exhibiting improved selectivity of ethylene.[8−10] In addition, a small amount of residual Br^- ions may adsorb on the surface of the catalyst and thus alter the catalytic performance of Cu. In most of the reported research, ethanol is a minor product in comparison with ethylene. The difficulty for ethanol production stems from the higher energy barrier for the formation of ethanol over ethylene and the scaling relationship restricting the adsorption energies of intermediates.[11]

The current strategy to improve the selectivity of ethanol typically relies on the introduction of a second metal element such as Au, Ag, and Zn, which modulates the surface coverage of *CO and thus promotes C−C coupling.[12−14] The selectivity of ethanol can be further improved by incorporating a specific metal oxide/hydroxide, such as $Ce(OH)_x$, to modulate *H coverage on the Cu surface.[15] Despite improved ethanol formation, these multicomponent catalysts suffer from the complicated synthetic process and delicate interfacial modulation. Therefore, a simple and efficient strategy without introducing other metal elements is highly desired to break the scaling relationship and improve the selectivity of ethanol.

Received: November 10, 2020
Accepted: December 14, 2020
Published: January 8, 2021

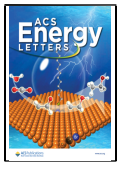

https://dx.doi.org/10.1021/acsenergylett.0c02364
ACS Energy Lett. 2021, 6, 437–444

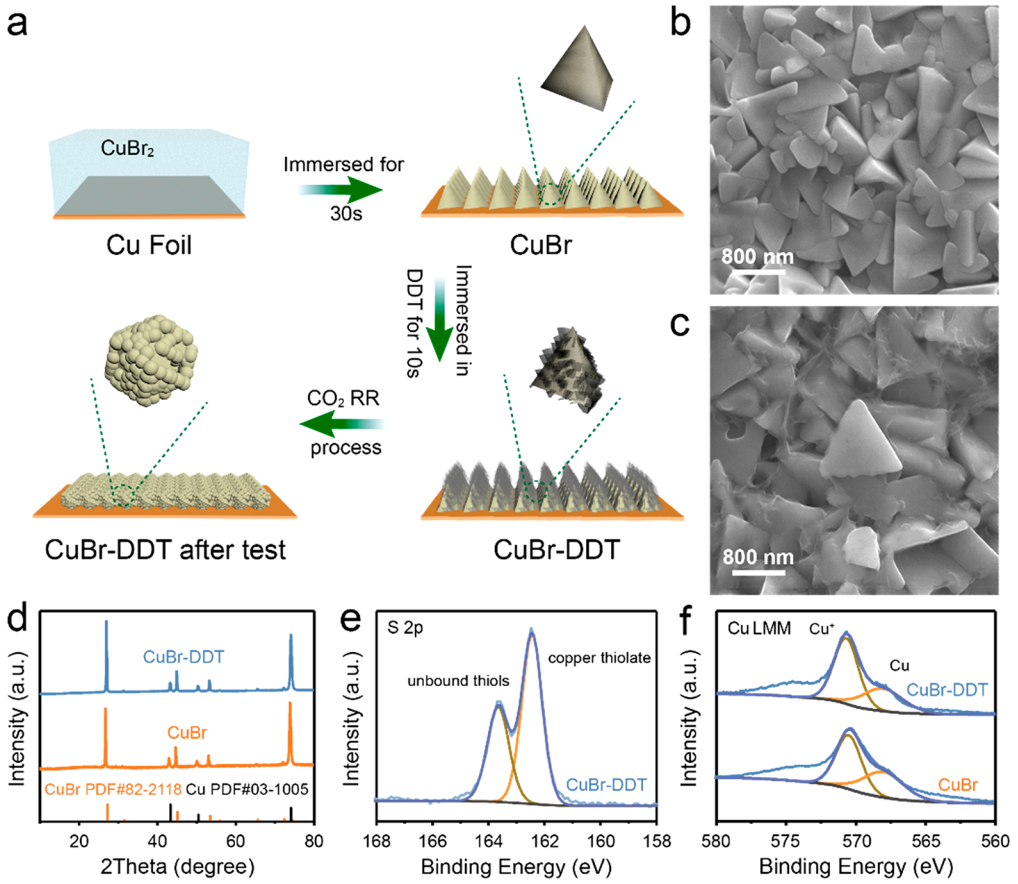

Figure 1. Synthesis and characterizations of DDT-modified CuBr. (a) Schematic of the synthetic process of CuBr-DDT (insets show the schematics of the microcrystals). (b and c) Top-view SEM images of CuBr and CuBr-DDT. (d) XRD profiles of CuBr and CuBr-DDT. (e) High-resolution S 2p XPS spectra and (f) XPS Cu LMM Auger spectra of CuBr and CuBr-DDT.

We envision that post C−C coupling selectivity could be steered on a properly designed metal−molecule interface. Modifying catalyst surfaces with organic molecules has been proven an effective strategy to optimize the hydrophobicity of catalysts and adsorption energies of intermediates.[16−21] The molecule-modified surface has been reported to suppress HER and, in turn, promote CO/ethylene formation.[18,20,22−24] However, manipulating the key reaction step toward other important oxygenates such as ethanol remains difficult. In principle, the high selectivity of ethanol requires both boosting the C−C coupling reaction and subsequent suppression of ethylene formation. In this work, we show that dodecanethiol-modified CuBr (termed CuBr-DDT) that *in situ* transforms into a Br-doped Cu−molecule interface, delivers improved ethanol selectivity and durability. Adsorption of hydrophobic dodecanethiol on CuBr also suppresses the parasitic HER. The advance of DDT, over the previous reported 1-octadecanethiol modifier, is its ability to steer the post-C−C coupling selectivity toward ethanol, instead of ethylene as previously reported.[23] Thus, the CuBr-DDT delivers highly promoted ethanol selectivity (35.9%) while suppressing hydrogen formation (10.1%). The performance of CuBr-DDT significantly surpasses those of pristine CuBr and many other Cu-based electrocatalysts. Furthermore, the CuBr-DDT electrocatalyst maintains high catalytic activity for over 15 h, much longer than that of the pristine CuBr, which deactivates within 2 h.

Figure 1a schematically illustrates the rapid and scalable synthetic process of CuBr nanotetrahedrons on Cu foil and subsequent dodecanethiol (DDT) modification. Typically, one piece of mechanically polished Cu foil was immersed in 0.1 M $CuBr_2$ solution for 30 s, leading to the rapid formation of CuBr tetrahedrons. The shiny red-brown color of mechanically polished Cu foil becomes pale after the reaction (Figure S1, in the Supporting Information). Visual inspection suggests the macroscopic uniformity of the resulting CuBr on Cu foil, and further modification of CuBr with DDT (denoted as CuBr-DDT) does not change the appearance of the sample. A scanning electron microscopy (SEM) analysis was performed to study the morphologies of CuBr and CuBr-DDT. Well-defined and closely packed tetrahedral nanostructures with a smooth surface are observed across the entire surface of the copper foil (Figure 1b). As shown in Figure 1c, the morphology is well-retained after treatment with DDT except for a slightly coarsened surface. In addition, floc-like features are observed on the surface of CuBr-DDT, which may be attributed to the surface-adsorbed DDT. To examine the spatial distribution of DDT on the surface of CuBr, elemental mapping using energy dispersive X-ray (EDX) spectroscopy was performed on an SEM instrument. As shown in Figure S2, evenly distributed elements of S, Cu, and Br suggest the uniform coverage of CuBr with DDT. The crystal phase of the sample was confirmed by the X-ray diffraction (XRD) pattern (Figure 1d). In addition to the peaks from metallic Cu, the major signals can be well-assigned to CuBr (PDF #82-2188)

https://dx.doi.org/10.1021/acsenergylett.0c02364
ACS Energy Lett. 2021, 6, 437−444

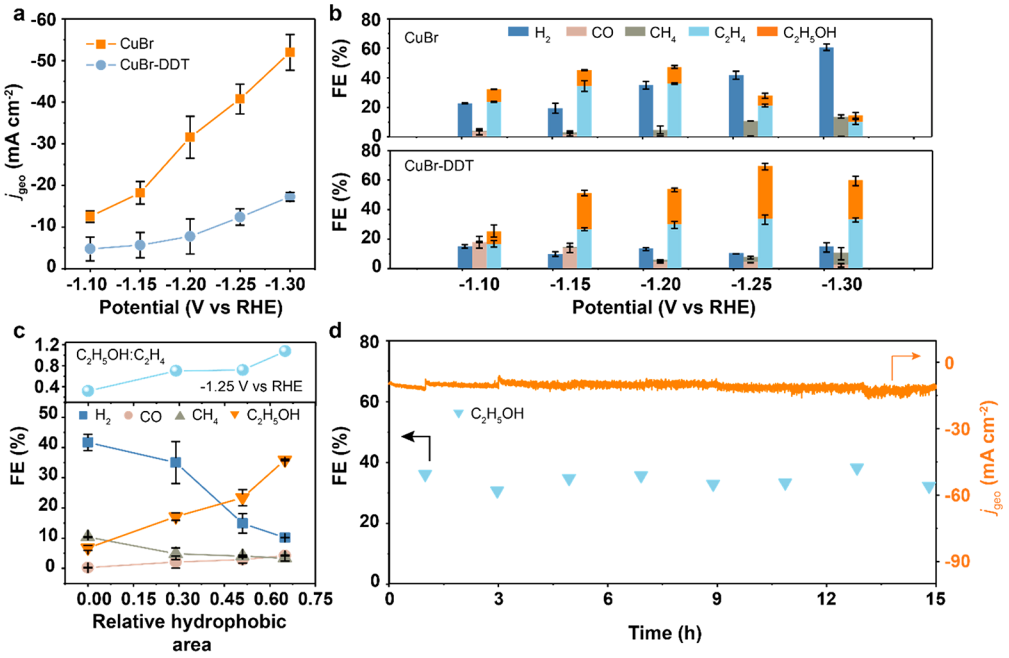

Figure 2. Electrochemical CO_2 reduction performance of CuBr-DDT. (a) Geometric-surface-area-normalized current densities of CO_2 reduction for CuBr and CuBr-DDT. (b) CO_2 reduction product FEs from the CuBr and CuBr-DDT at various potentials. (c) The ratio of ethanol/ethylene (upper panel) and product distribution (lower panel) on CuBr-DDT as a function of the relative hydrophobic area. (d) *i*–*t* curve (right axis) of CuBr-DDT along with corresponding Faradaic efficiency of ethanol (left axis).

with high crystallinity, suggesting the presence of a relatively thick CuBr layer on Cu foil. There is no noticeable change in the XRD pattern after modifying with DDT. To probe the presence of DDT and its interaction with CuBr, X-ray photoelectron spectroscopy (XPS) was performed. The S 2p peak positions located at 162.4 and 163.5 eV can be assigned to copper thiolate and unbound thiols, respectively (Figure 1e).[25] The stronger peak intensity of copper thiolate than that of unbound thiols indicates most DDT molecules are bound with copper. The Cu LMM Auger signal was further analyzed to study the impact of DDT on the electronic structure of Cu (Figure 1f). CuBr-DDT possesses a very similar Cu LMM Auger signal compared to CuBr, indicating the unchanged valence of Cu(I) in the sample.

The activity of CuBr-DDT and CuBr for CO_2RR was assessed by potentiostatic measurements for 60 min at selected potentials from −1.1 to −1.3 V (vs RHE) in a gastight H-type glass cell separated by a Nafion 117 membrane. The current densities of CuBr normalized by geometric surface area are decreased after the modification of DDT as shown in Figure 2a. Given that the adsorption of hydrophobic DDT would partially cover the active sites and repel the electrolyte, the electrochemically active surface area (ECSA) is estimated by measuring the electrical double-layer capacitance (EDLC).[23] The ECSA of CuBr-DDT represented by EDLC is notably reduced from 1.44 cm^2 for pristine CuBr to 0.51 cm^2 for CuBr-DDT because of the formation of a hydrophobic surface (Figure S3). To compare the intrinsic activity, the total current densities and CO_2RR partial current densities of CuBr and CuBr-DDT were normalized by ECSA (Figure S4). Interestingly, while the total current densities of CuBr and CuBr-DDT exhibit a similar trend, the partial current densities of CO_2 electroreduction are different. The CO_2RR partial current density of CuBr reaches the maximum at −1.25 V (vs RHE), whereas that of CuBr-DDT increases with the applied potential. CuBr-DDT achieves a high CO_2RR ECSA-normalized partial current density of 28.9 mA cm^{-2} at −1.3 V (vs RHE), about two times larger than that of CuBr.

In addition to the change of current density, modification of CuBr with DDT has a significant influence on the distributions of CO_2RR products (Figure 2b). Major products, including H_2 from parasitic water reduction, were detected, and specific product distributions are shown in Tables S1 and S2. Important observations on the change of product distributions are summarized below:

(i) Compared with CuBr, HER on CuBr-DDT is dramatically suppressed, especially under large overpotential. CuBr-DDT maintains a relatively low FE of H_2 (∼10%) over a wide range of tested potential. In contrast, the selectivity of H_2 on CuBr increases quickly as the potential is more negative (FE_{H_2} = 60.5% at −1.3 V). It is worth noting that the H_2 selectivity of CuBr is apparently higher than that of CuBr-DDT even operated under similar current densities (Figure S5).

(ii) In terms of C1 gaseous products, CuBr achieves a negligible CO selectivity. In contrast, CuBr-DDT exhibits a much higher selectivity for CO (FE_{CO} = 17.6% at 1.1 V vs RHE), about five times higher than that of CuBr. Meanwhile, the formation of CH_4, which consumes intermediate CO before the C−C coupling reaction occurs, is effectively suppressed on CuBr-DDT under the small potentials (<1.3 V vs RHE) compared to that on CuBr.

(iii) The C2 product distributions of CuBr-DDT are also different from that of CuBr. In line with the previous report,[8] CuBr reaches the maximum $FE_{C_2H_4}$ of 35.9% at −1.2 V vs RHE, and the total FE of C2 product approaches 47%. At high overpotential, the FE of C2 products decreases significantly (FE_{C2} = 27.7 and 14.4% at −1.25 and −1.30 V, respectively). For CuBr-DDT, a high FE for ethylene of 33.3% is achieved at −1.25 V vs RHE, comparable to the maximal value obtained by CuBr. More interestingly, the FE of ethanol is greatly improved

https://dx.doi.org/10.1021/acsenergylett.0c02364
ACS Energy Lett. 2021, 6, 437−444

to 35.9%, which is about 5.4 times greater than that of CuBr under the same applied potential and 2 times greater than that of 1-octadecanethiol modified Cu dendrites as reported previously.[23] It is worth noting that CuBr-DDT gives a large ECSA-normalized ethanol partial current density of 8.75 mA cm^{-2}, much better than that of CuBr. In addition, CuBr-DDT gives a high half-cell cathodic energy efficiency of 16.6% toward ethanol, an important indicator to evaluate the catalyst, about 5 times greater than that of CuBr (Figure S6). To the best of our knowledge, this is one of the most selective and active electrocatalysts for producing ethanol reported to date (Figure S27 and Table S3).

The structure and morphology of CuBr and CuBr-DDT were examined after CO_2RR to understand the different catalytic performance. XRD patterns (Figure S7) show that both CuBr and CuBr-DDT are reduced to Cu after the electrocatalytic reaction because of the negative potential applied. Interestingly, CuBr and CuBr-DDT exhibit distinctive morphologies after CO_2RR. For CuBr, nanoparticles are assembled into dendrite-like nanostructures with no detectable Br signal from EDX (Figure S8), which is consistent with a previous report.[8] Instead, irregular nanoparticle assemblies are observed in CuBr-DDT (Figure S9a). The different morphologies can be attributed to the presence of DDT, which hinders the migration of Br^- ions from the bulk of CuBr to the solution. Such a hypothesis is further supported by the detection of Br in CuBr-DDT after electrocatalytic CO_2 reduction (Figure S9b). In addition, to exclude the effect of current density on the morphology evolution, CuBr is tested at a constant current density of −10 mA cm^{-2}. Similar dendrite-like nanostructures can be observed (Figure S10), confirming that DDT plays a key role in preventing dendrite formation. Meanwhile, the residual Br^-, together with adsorbed DDT, would play an important role in modulating the catalytic behavior of Cu catalyst, as discussed shortly.

Given that the amount of Br-doped Cu−molecule interface is proportional to the hydrophobic area (surface with adsorbed DDT), we control the amount of adsorbed DDT on CuBr by using DDT/isopropanol solution to quantify the impact of Br-doped Cu−molecule interface on the CO_2RR activity. The amount of residual Br^- ions is found to be proportional to the surface adsorbed DDT (Figure S11). Figure 2c shows the ratio of ethanol-to-ethylene (upper panel) and the gas product distribution (lower panel) of various DDT-modified CuBr samples at −1.25 V vs RHE as a function of the relative hydrophobic area. The relative hydrophobic area is defined as the reduced ECSA after DDT modification with respect to the ECSA of pristine CuBr (Figure S3c). As the relative hydrophobic area increases, the ratio of ethanol-to-ethylene increases from 0.32 to 1.08, and the selectivity of ethanol increases from 6.7% to 35.9%. In addition, HER activity is suppressed with the increase of the relative hydrophobic area. The selectivity of CH_4 shows the same tendency, implying that both methane and hydrogen are dependent on proton concentration which is actively linked to the hydrophobicity.

Durability represents another critical issue for electrocatalysts. The catalytic stability of CuBr-DDT was evaluated at −1.25 V vs RHE (Figures 2d and S12). The FEs of various products and the corresponding current density were maintained during the operating period of 15 h, indicating good stability for CuBr-DDT. In addition, contact angle measurements illustrate that the hydrophobic feature remains after 15 h of electrolysis, demonstrating the robust binding of DDT on the surface of CuBr (Figure S13). In sharp contrast, CuBr exhibits rapid degradation at −1.2 V vs RHE, a milder operation condition (Figure S14). The FE of ethylene for CuBr increases in the first hour and then decreases quickly, whereas the FE of H_2 keeps increasing. Moreover, at a fixed current density operation of 20 mA cm^{-2}, which is closed to the current density of CuBr-DDT, the performance of CuBr also quickly deteriorates (Figure S15). Thus, modification of DDT would improve both the catalytic activity and the durability of the electrocatalyst.

To investigate the role of residual Br^-, CuBr was first reduced to metallic Cu by cyclic voltammetry (CV) scans (denoted as CuBr-CV). SEM images show that the CuBr tetrahedrons were converted to Cu nanoparticles after CV (Figure S16), and no remaining Br^- is detected by EDX (Figure S17). After a similar DDT modification process, the electrode (denoted as CuBr-CV-DDT) with an undoped Cu-DDT interface (Figures S18 and S19) is subjected to CO_2RR test at various potentials. The selectivity of ethanol for CuBr-CV-DDT is higher than that of CuBr but apparently lower than that of CuBr-DDT (Figure S20), suggesting that a synergy between Br^- ions and copper-DDT interface may exist, and Br^- plays a more key role than DDT in modulating the catalytic pathway of ethanol. In addition, the FE of ethylene drastically drops in the first half-hour and constantly decreases afterward, whereas the FE of hydrogen rises rapidly during a 4 h test (Figure S21). Postcycle analysis reveals a dendrite-like morphology similar to that of postcycled CuBr (Figure S22) with most of the DDT molecules being removed (Figure S23). Therefore, the presence of Br^- is critically important to stabilize the metal−molecule interface. Fourier transform infrared (FT-IR) spectra were collected to support this conjecture (Figure S24). Two bands due to asymmetric and symmetric methylene stretching in DDT are observed at 2920 and 2850 cm^{-1}, respectively. After CO_2 electrolysis, these two bands remain, providing a solid evidence for the excellent robustness of the Br-doped Cu-DDT structure.

Density function theory (DFT) calculations were carried out to investigate the reaction mechanism and the influence of DDT by calculating the elementary reactions. Two surface models were considered in the calculation: one is pure Cu (111) surface, the dominant surface of the Cu-based catalysts (Figure S25), and the other is a modified Cu(111) to stand for CuBr-DDT. The modified Cu (111) model consists of a 4 × 4 × 3 Cu(111) surface slab model with one sublayer Cu atom replaced by Br atom. The chemisorbed surfactant was simulated by introducing one 1-propanethiol with the S chemically bonded on the Cu surface. The three-carbon chain represents high computation efficiency while maintaining the main feature of the experiment. For example, using this CuBr-DDT simulation model, we calculated the 3p core level of Cu and predict a chemical shift of 72.23 eV for Cu directly in contact with Br. Taking the 71.42 eV of pure Cu (Cu^0) and 72.45 eV of Cu_2O (Cu^+), it is clear that interested Cu sites in CuBr-DDT are close to 1+, which is in line with the experimental characterization that verified the presence and the important role of Cu^+ in improving the performance.

We first investigate HER performance by calculating the hydrogen binding energy. The DFT calculation shows that the adsorption of hydrogen on the Br-doped Cu surface with thiol modification is significantly suppressed compared with that of the bare Br-doped Cu surface (Figure S26). It is known that

https://dx.doi.org/10.1021/acsenergylett.0c02364
ACS Energy Lett. 2021, 6, 437−444

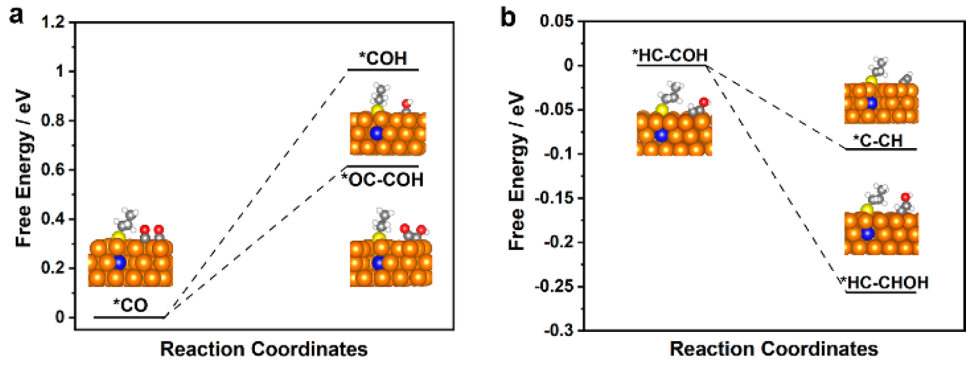

Figure 3. DFT simulation of energy profiles of key reaction steps and optimized atomic structures. (a) The free energy differences of *COH and *OCCOH formation and the optimized adsorption structures of *CO, *COH, and *OC−COH on CuBr-DDT, respectively. (b) The free energy differences of *C−CH and *HC−CHOH formation and the optimized adsorption structures of *HC−COH, *C−CH, and *HC−CHOH on CuBr-DDT, respectively.

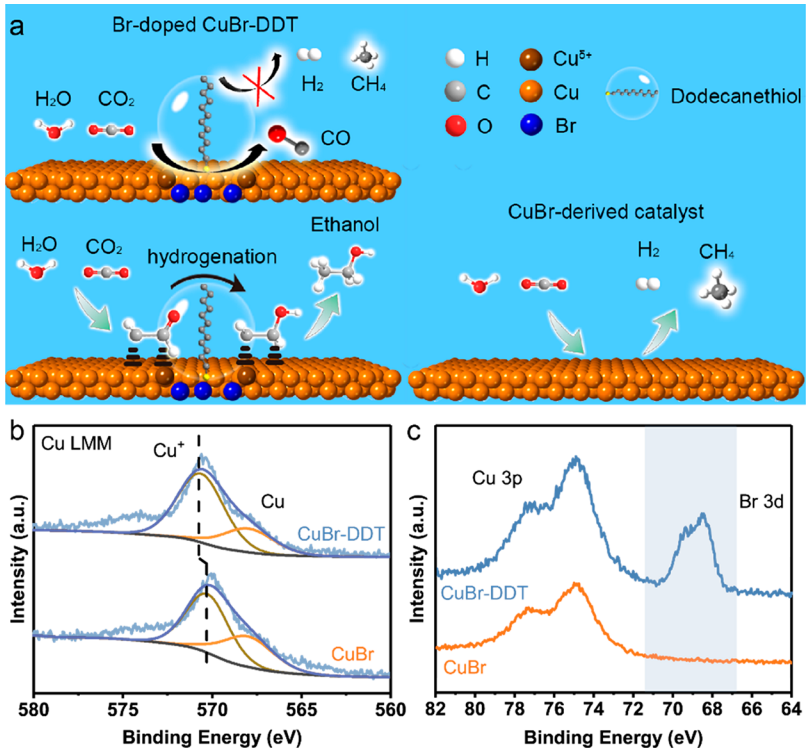

Figure 4. Atomic structure and catalytic mechanism on CuBr-DDT. (a) Schematic of CO_2 RR process for CuBr-DDT and CuBr-derived catalyst. XPS Cu LMM Auger (b) and high-resolution Br 3d XPS spectra (c) of CuBr and CuBr-DDT after electrocatalytic CO_2RR at −1.25 V (vs RHE) for 1 h.

decreasing the hydrogen binding energy of Cu suppresses HER. Such a prediction is consistent with the experiment.

Then, we focused on the competition between C1 and C2, by considering the potential-determining steps (PDSs) of C1 and C2 products, which are the formation of *COH in C1 formation, and *OC−COH formation in C2 formation.[26] The difference in the formation energies of *COH and *OC−COH was employed as the descriptor to distinguish the preference of C1 and C2 products. For CuBr-DDT, the formation energy of *OC−COH is 0.61 eV, 0.42 eV lowered than that of *COH (1.03 eV), as shown in Figure 3a, which indicates that C2 formation is more favorable on CuBr-DDT over C1 product. Such prediction is also consistent with experimental observation.

The final question is the selectivity between ethylene and ethanol. In our previous research, we found that ethylene and ethanol share the same common intermediate but branch in the stage after *OC−COH formation. Despite the existing dispute, *HC−COH has been previously distinguished as the most possible intermediates determining the selectivity between ethylene and ethanol.[11,27] Therefore, the competition between these two reactions from *HC−COH indicates the preference of ethylene or ethanol formation. Specifically, *HC−COH can be reduced to *HC−CHOH leading to ethanol or *C−CH leading to ethylene. Our DFT calculations on both Cu(111) and CuBr-DDT show that the thiol adsorbate significantly lowers the formation energy of *HC−CHOH (precursor to ethanol) by 0.16 eV with respect to *C−CH (precursor to ethylene) on the surface representing CuBr-

https://dx.doi.org/10.1021/acsenergylett.0c02364
ACS Energy Lett. 2021, 6, 437−444

DDT (Figure 3b), suggesting that CuBr-DDT promotes ethanol formation and in turn suppresses ethylene formation. The DFT result provides a plausible explanation for the favored ethanol formation on CuBr-DDT, while further in-depth study is necessary to reveal the mechanism.

Combining experimental and DFT calculations, the surface structure and mechanism of CO_2RR on thiol-modified CuBr is schematically summarized in Figure 4a. Specifically, DDT adsorbed on CuBr creates a unique Br-doped Cu−thiol interface with high stability during the catalytic process, where the residual Br^- and adsorbed DDT are mutually stabilized by each other. The adsorption of DDT decreases the coverage of *H, suppressing the product selectivity of both hydrogen and methane. Note that the incorporation of Br^- species in Cu would change the electron structure (*e.g.*, forming copper with positive valence sites because of charge compensation) and thus steer the selectivity toward C2 products, especially ethanol. Although some experimental and theoretical works have cast significant doubt on the existence of residual oxide and Cu^+ during CO_2RR,[28−31] copper with positive valence sites ($Cu^{\delta+}$) might be stabilized during CO_2RR by specific strategies (*e.g.*, doping elements with high electronegativity) and promotes the formation of C2 products.[32−35] *Ex situ* XPS was conducted on CuBr and CuBr-DDT to investigate the valence and composition after CO_2 RR. While the signal assigned to Cu^+ at around 570 eV is available on the Cu LMM Auger spectra of both samples, the peak shifts toward higher binding energy in postcycled CuBr-DDT (Figure 4b). The shifted binding energy of Cu^+ can be attributed to the strong electronegativity of Br^- ions. The signal of Br^- can be well-recognized by XPS (Figure 4c), confirming the presence of Br^- in the surface and/or near-surface region, thus significantly modulating the surface catalytic properties. Moreover, we predict with DFT calculations that the 3p core level of Cu near Br in our computational model is 72.23 eV, very close to that of Cu^+ in Cu_2O (72.45 eV) but different from that of Cu^0 (71.42 eV). Thus, both experimental and computational results are in good agreement, supporting the presence of $Cu^{\delta+}$ and its influence on CO_2 conversion on the Br-doped Cu−thiol interface.

In summary, we report a convenient and effective strategy to increase the selectivity of electrochemically reducing CO_2 toward C2 products, especially ethanol on the *in situ* formed metal−molecule interface doped with halide ions. Experimental results show that CuBr modified with DDT molecules delivers a high Faradaic efficiency of 72% for C2+ products and a high ethanol-to-ethylene ratio, close to 1.1. Adsorption of DDT on CuBr might hinder the migration of Br^- and complete reduction of CuBr, thus creating a unique Br-doped Cu−thiol interface with high stability during the catalytic process. The mechanistic study indicates that the adsorption of DDT suppresses the product selectivity of hydrogen and methane. Incorporation of Br^- species in Cu would stabilize high-valence Cu species and thus steer the selectivity toward C2 products, especially ethanol. Constructing a robust metal−molecule interface with doped anionic species opens up a new route to engineer the intermediate distributions on the catalyst surface and thus to modulate product selectivity. We believe that such a strategy would shed light on the design of other electrocatalytic systems involving complex electron−proton-transfer processes.

■ ASSOCIATED CONTENT

Supporting Information

The Supporting Information is available free of charge at https://pubs.acs.org/doi/10.1021/acsenergylett.0c02364.

Experimental details, SEM, EDX-mapping, XRD, and other electrochemical measurements (PDF)

■ AUTHOR INFORMATION

Corresponding Authors

Tao Cheng − *Institute of Functional Nano & Soft Materials (FUNSOM), Jiangsu Key Laboratory for Carbon-Based Functional Materials & Devices, Soochow University, Jiangsu 215123, China;* orcid.org/0000-0003-4830-177X; Email: tcheng@suda.edu.cn

Hao Bin Wu − *Institute for Composites Science Innovation (InCSI), School of Materials Science and Engineering, Zhejiang University, Hangzhou 310027, China;* orcid.org/0000-0002-0725-6442; Email: hbwu@zju.edu.cn

Authors

Jianghao Wang − *Institute for Composites Science Innovation (InCSI), School of Materials Science and Engineering, Zhejiang University, Hangzhou 310027, China*

Hao Yang − *Institute of Functional Nano & Soft Materials (FUNSOM), Jiangsu Key Laboratory for Carbon-Based Functional Materials & Devices, Soochow University, Jiangsu 215123, China;* orcid.org/0000-0002-8241-6231

Qianqian Liu − *Institute for Composites Science Innovation (InCSI), School of Materials Science and Engineering, Zhejiang University, Hangzhou 310027, China*

Qian Liu − *Institute for Composites Science Innovation (InCSI), School of Materials Science and Engineering, Zhejiang University, Hangzhou 310027, China*

Xiaotong Li − *Institute for Composites Science Innovation (InCSI), School of Materials Science and Engineering, Zhejiang University, Hangzhou 310027, China*

Xiangzhou Lv − *Institute for Composites Science Innovation (InCSI), School of Materials Science and Engineering, Zhejiang University, Hangzhou 310027, China*

Complete contact information is available at: https://pubs.acs.org/10.1021/acsenergylett.0c02364

Author Contributions

§J.W. and H.Y. contributed equally.

Notes

The authors declare no competing financial interest.

■ ACKNOWLEDGMENTS

H.B.W. acknowledges the funding support from "Hundred Talents Program" of Zhejiang University. T.C. was supported by the National Natural Science Foundation of China (Grant No. 21903058), the Fundamental Research Funds for the Central Universities, the Natural Science Foundation of Jiangsu Province (Grant No. BK20190810), and Jiangsu Province High-Level Talents (JNHB-106). H.Y. was supported by China Postdoctoral Science Foundation (No. 2019M660128). T.C. was partly supported by the Collaborative Innovation Center of Suzhou Nano Science & Technology, the Priority Academic Program Development of Jiangsu Higher Education Institutions (PAPD), and the 111 Project.

REFERENCES

(1) Hori, Y.; Murata, A.; Takahashi, R. Formation of Hydrocarbons in the Electrochemical Reduction of Carbon Dioxide at a Copper Electrode in Aqueous Solution. *J. Chem. Soc., Faraday Trans. 1* **1989**, *85* (8), 2309−2326.

(2) Hori, Y.; Murata, A.; Yoshinami, Y. Adsorption of CO, Intermediately Formed in Electrochemical Reduction of CO_2, at a Copper Electrode. *J. Chem. Soc., Faraday Trans.* **1991**, *87* (1), 125−128.

(3) Hori, Y.; Takahashi, R.; Yoshinami, Y.; Murata, A. Electrochemical Reduction of CO at a Copper Electrode. *J. Phys. Chem. B* **1997**, *101* (36), 7075−7081.

(4) Zhang, W.; Hu, Y.; Ma, L.; Zhu, G.; Wang, Y.; Xue, X.; Chen, R.; Yang, S.; Jin, Z. Progress and Perspective of Electrocatalytic CO_2 Reduction for Renewable Carbonaceous Fuels and Chemicals. *Advanced Science* **2018**, *5* (1), 1700275.

(5) Nitopi, S.; Bertheussen, E.; Scott, S. B.; Liu, X.; Engstfeld, A. K.; Horch, S.; Seger, B.; Stephens, I. E. L.; Chan, K.; Hahn, C.; Nørskov, J. K.; Jaramillo, T. F.; Chorkendorff, I. Progress and Perspectives of Electrochemical CO_2 Reduction on Copper in Aqueous Electrolyte. *Chem. Rev.* **2019**, *119* (12), 7610−7672.

(6) Resasco, J.; Bell, A. T. Electrocatalytic CO_2 Reduction to Fuels: Progress and Opportunities. *Trends in Chemistry* **2020**, *2* (9), 825−836.

(7) Yano, H.; Tanaka, T.; Nakayama, M.; Ogura, K. Selective Electrochemical Reduction of CO_2 to Ethylene at a Three-Phase Interface on Copper(I) Halide-Confined Cu-Mesh Electrodes in Acidic Solutions of Potassium Halides. *J. Electroanal. Chem.* **2004**, *565* (2), 287−293.

(8) Wang, H.; Matios, E.; Wang, C.; Luo, J.; Lu, X.; Hu, X.; Li, W. Rapid and Scalable Synthesis of Cuprous Halide-Derived Copper Nano-Architectures for Selective Electrochemical Reduction of Carbon Dioxide. *Nano Lett.* **2019**, *19* (6), 3925−3932.

(9) Gao, D.; Sinev, I.; Scholten, F.; Arán-Ais, R. M.; Divins, N. J.; Kvashnina, K.; Timoshenko, J.; Roldan Cuenya, B. Selective CO_2 Electroreduction to Ethylene and Multicarbon Alcohols via Electrolyte-Driven Nanostructuring. *Angew. Chem., Int. Ed.* **2019**, *58* (47), 17047−17053.

(10) Kim, T.; Palmore, G. T. R. A Scalable Method for Preparing Cu Electrocatalysts That Convert CO_2 into C2+ Products. *Nat. Commun.* **2020**, *11* (1), 3622.

(11) Garza, A. J.; Bell, A. T.; Head-Gordon, M. Mechanism of CO_2 Reduction at Copper Surfaces: Pathways to C2 Products. *ACS Catal.* **2018**, *8* (2), 1490−1499.

(12) Li, Y. C.; Wang, Z.; Yuan, T.; Nam, D.-H.; Luo, M.; Wicks, J.; Chen, B.; Li, J.; Li, F.; de Arquer, F. P. G.; Wang, Y.; Dinh, C.-T.; Voznyy, O.; Sinton, D.; Sargent, E. H. Binding Site Diversity Promotes CO_2 Electroreduction to Ethanol. *J. Am. Chem. Soc.* **2019**, *141* (21), 8584−8591.

(13) Shen, S.; Peng, X.; Song, L.; Qiu, Y.; Li, C.; Zhuo, L.; He, J.; Ren, J.; Liu, X.; Luo, J. AuCu Alloy Nanoparticle Embedded Cu Submicrocone Arrays for Selective Conversion of CO_2 to Ethanol. *Small* **2019**, *15* (37), 1902229.

(14) Ren, D.; Gao, J.; Pan, L.; Wang, Z.; Luo, J.; Zakeeruddin, S. M.; Hagfeldt, A.; Grätzel, M. Atomic Layer Deposition of ZnO on CuO Enables Selective and Efficient Electroreduction of Carbon Dioxide to Liquid Fuels. *Angew. Chem., Int. Ed.* **2019**, *58* (42), 15036−15040.

(15) Luo, M.; Wang, Z.; Li, Y. C.; Li, J.; Li, F.; Lum, Y.; Nam, D.-H.; Chen, B.; Wicks, J.; Xu, A.; Zhuang, T.; Leow, W. R.; Wang, X.; Dinh, C.-T.; Wang, Y.; Wang, Y.; Sinton, D.; Sargent, E. H. Hydroxide Promotes Carbon Dioxide Electroreduction to Ethanol on Copper via Tuning of Adsorbed Hydrogen. *Nat. Commun.* **2019**, *10* (1), 1−7.

(16) Li, F.; Thevenon, A.; Rosas-Hernández, A.; Wang, Z.; Li, Y.; Gabardo, C. M.; Ozden, A.; Dinh, C. T.; Li, J.; Wang, Y.; Edwards, J. P.; Xu, Y.; McCallum, C.; Tao, L.; Liang, Z.-Q.; Luo, M.; Wang, X.; Li, H.; O'Brien, C. P.; Tan, C.-S.; Nam, D.-H.; Quintero-Bermudez, R.; Zhuang, T.-T.; Li, Y. C.; Han, Z.; Britt, R. D.; Sinton, D.; Agapie, T.; Peters, J. C.; Sargent, E. H. Molecular Tuning of CO_2-to-Ethylene Conversion. *Nature* **2020**, *577* (7791), 509−513.

(17) Pankhurst, J. R.; Guntern, Y. T.; Mensi, M.; Buonsanti, R. Molecular Tunability of Surface-Functionalized Metal Nanocrystals for Selective Electrochemical CO_2 Reduction. *Chem. Sci.* **2019**, *10* (44), 10356−10365.

(18) Xie, M. S.; Xia, B. Y.; Li, Y.; Yan, Y.; Yang, Y.; Sun, Q.; Chan, S. H.; Fisher, A.; Wang, X. Amino Acid Modified Copper Electrodes for the Enhanced Selective Electroreduction of Carbon Dioxide towards Hydrocarbons. *Energy Environ. Sci.* **2016**, *9* (5), 1687−1695.

(19) Ahn, S.; Klyukin, K.; Wakeham, R. J.; Rudd, J. A.; Lewis, A. R.; Alexander, S.; Carla, F.; Alexandrov, V.; Andreoli, E. Poly-Amide Modified Copper Foam Electrodes for Enhanced Electrochemical Reduction of Carbon Dioxide. *ACS Catal.* **2018**, *8* (5), 4132−4142.

(20) Wei, X.; Yin, Z.; Lyu, K.; Li, Z.; Gong, J.; Wang, G.; Xiao, L.; Lu, J.; Zhuang, L. Highly Selective Reduction of CO_2 to C2+ Hydrocarbons at Copper/Polyaniline Interfaces. *ACS Catal.* **2020**, *10* (7), 4103−4111.

(21) Lau, G. P. S.; Schreier, M.; Vasilyev, D.; Scopelliti, R.; Grätzel, M.; Dyson, P. J. New Insights Into the Role of Imidazolium-Based Promoters for the Electroreduction of CO_2 on a Silver Electrode. *J. Am. Chem. Soc.* **2016**, *138* (25), 7820−7823.

(22) Buckley, A. K.; Lee, M.; Cheng, T.; Kazantsev, R. V.; Larson, D. M.; Goddard, W. A., III; Toste, F. D.; Toma, F. M. Electrocatalysis at Organic−Metal Interfaces: Identification of Structure−Reactivity Relationships for CO_2 Reduction at Modified Cu Surfaces. *J. Am. Chem. Soc.* **2019**, *141* (18), 7355−7364.

(23) Wakerley, D.; Lamaison, S.; Ozanam, F.; Menguy, N.; Mercier, D.; Marcus, P.; Fontecave, M.; Mougel, V. Bio-Inspired Hydrophobicity Promotes CO_2 Reduction on a Cu Surface. *Nat. Mater.* **2019**, *18* (11), 1222−1227.

(24) Cao, Z.; Kim, D.; Hong, D.; Yu, Y.; Xu, J.; Lin, S.; Wen, X.; Nichols, E. M.; Jeong, K.; Reimer, J. A.; Yang, P.; Chang, C. J. A Molecular Surface Functionalization Approach to Tuning Nanoparticle Electrocatalysts for Carbon Dioxide Reduction. *J. Am. Chem. Soc.* **2016**, *138* (26), 8120−8125.

(25) Dilimon, V. S.; Denayer, J.; Delhalle, J.; Mekhalif, Z. Electrochemical and Spectroscopic Study of the Self-Assembling Mechanism of Normal and Chelating Alkanethiols on Copper. *Langmuir* **2012**, *28* (17), 6857−6865.

(26) Cheng, T.; Xiao, H.; Goddard, W. A. Full Atomistic Reaction Mechanism with Kinetics for CO Reduction on Cu (100) from Ab Initio Molecular Dynamics Free-Energy Calculations at 298 K. *Proc. Natl. Acad. Sci. U. S. A.* **2017**, *114* (8), 1795−1800.

(27) Cheng, T.; Fortunelli, A.; Goddard, W. A. Reaction Intermediates during Operando Electrocatalysis Identified from Full Solvent Quantum Mechanics Molecular Dynamics. *Proc. Natl. Acad. Sci. U. S. A.* **2019**, *116* (16), 7718−7722.

(28) Fields, M.; Hong, X.; Nørskov, J. K.; Chan, K. Role of Subsurface Oxygen on Cu Surfaces for CO_2 Electrochemical Reduction. *J. Phys. Chem. C* **2018**, *122* (28), 16209−16215.

(29) Garza, A. J.; Bell, A. T.; Head-Gordon, M. Is Subsurface Oxygen Necessary for the Electrochemical Reduction of CO_2 on Copper? *J. Phys. Chem. Lett.* **2018**, *9* (3), 601−606.

(30) Scott, S. B.; Hogg, T. V.; Landers, A. T.; Maagaard, T.; Bertheussen, E.; Lin, J. C.; Davis, R. C.; Beeman, J. W.; Higgins, D.; Drisdell, W. S.; Hahn, C.; Mehta, A.; Seger, B.; Jaramillo, T. F.; Chorkendorff, I. Absence of Oxidized Phases in Cu under CO Reduction Conditions. *ACS Energy Lett.* **2019**, *4* (3), 803−804.

(31) Lum, Y.; Ager, J. W. Stability of Residual Oxides in Oxide-Derived Copper Catalysts for Electrochemical CO_2 Reduction Investigated with ^{18}O Labeling. *Angew. Chem., Int. Ed.* **2018**, *57* (2), 551−554.

(32) Bai, X.; Li, Q.; Shi, L.; Niu, X.; Ling, C.; Wang, J. Hybrid Cu^0 and Cu^{x+} as Atomic Interfaces Promote High-Selectivity Conversion of CO_2 to C_2H_5OH at Low Potential. *Small* **2020**, *16* (12), 1901981.

(33) Arán-Ais, R. M.; Scholten, F.; Kunze, S.; Rizo, R.; Roldan Cuenya, B. The Role of in Situ Generated Morphological Motifs and Cu(i) Species in C2+ Product Selectivity during CO_2 Pulsed Electroreduction. *Nat. Energy* **2020**, *5* (4), 317−325.

https://dx.doi.org/10.1021/acsenergylett.0c02364
ACS Energy Lett. 2021, 6, 437−444

(34) Zhou, Y.; Che, F.; Liu, M.; Zou, C.; Liang, Z.; Luna, P. D.; Yuan, H.; Li, J.; Wang, Z.; Xie, H.; Li, H.; Chen, P.; Bladt, E.; Quintero-Bermudez, R.; Sham, T.-K.; Bals, S.; Hofkens, J.; Sinton, D.; Chen, G.; Sargent, E. H. Dopant-Induced Electron Localization Drives CO_2 Reduction to C2 Hydrocarbons. *Nat. Chem.* **2018**, *10* (9), 974.

(35) He, M.; Li, C.; Zhang, H.; Chang, X.; Chen, J. G.; Goddard, W. A.; Cheng, M.; Xu, B.; Lu, Q. Oxygen Induced Promotion of Electrochemical Reduction of CO_2 via Co-Electrolysis. *Nat. Commun.* **2020**, *11* (1), 3844.

https://dx.doi.org/10.1021/acsenergylett.0c02364
ACS Energy Lett. 2021, 6, 437−444